Chapter 8
Metal-Induced Energy Transfer Imaging

Alexey I. Chizhik and Jörg Enderlein

Abstract Super-resolution microscopy has seen a tremendous development over the last two decades. It has opened new perspectives for the application of fluorescence microscopy in the life sciences. Achieving a spatial resolution beyond the diffraction limit of light allowed one to observe many biological structures that are not resolvable in conventional fluorescence microscopy. However, despite recent development of super-resolution fluorescence microscopy techniques that allowed for squeezing the lateral resolution down to tens of nanometers, the much less axial resolution remains a key limiting factor for applications where z-sectioning of a sample is needed. In this chapter, we present the recently developed fluorescence imaging method that is called metal-induced energy transfer. It combines unprecedented nanometer resolution with technical simplicity that allows life science researchers to use it with standard microscopes. We discuss basic principle of the method, its theoretical background, and its applications for imaging of various sub-cellular structures.

PACS Subject Classification: 87.64.M- · 73.20.Mf

8.1 Introduction

Fluorescence imaging is one of the most commonly used techniques for investigation of biological systems. Among its key advantages are (i) possibility to observe live samples in real time, (ii) the technical simplicity that makes it accessible for a broad community of life-science researchers, and (iii) specific labeling allows one to directly visualize sub-cellular structures. However, the wave nature of light limits the spatial resolution of a conventional fluorescence microscope, i.e. it cannot resolve structures smaller than the diffraction-limit. In the visible spectral range, this

A. I. Chizhik (✉) · J. Enderlein
Third Institute of Physics - Biophysics, Universität Göttingen, Friedrich-Hund-Platz 1, 37077 Göttingen, Germany
e-mail: alexey.chizhik@phys.uni-goettingen.de

J. Enderlein
e-mail: jenderl@gwdg.de

T. Salditt et al. (eds.), *Nanoscale Photonic Imaging*, Topics in Applied Physics 134,
https://doi.org/10.1007/978-3-030-34413-9_8

corresponds to a spatial resolution of roughly half a micrometer along the optical (z-) axis, and of about a quarter of a micrometer in the xy-plane. The field of super-resolution microscopy has seen a tremendous development over the last two decades and has opened up new advances for the application of fluorescence microscopy in bio-imaging. However, each of the existing methods are either technically challenging and require high light excitation intensities at the limit of what is tolerable for live-cell imaging, or are rather slow and require specialized labels and environmental conditions, which are not always compatible with live-cell microscopy. Moreover, the majority of these methods suffer from one common problem: Their axial resolution is by roughly one order of magnitude worse than their lateral resolution.

In this chapter, we present a new fluorescence-based method called metal-induced energy transfer (MIET), which is based on the energy transfer from an optically excited donor molecule to a thin metal film. It allows one to achieve an axial localization of a fluorophore with down to one nanometer accuracy. This goes far beyond the diffraction limit of light microscopy and surpasses in accuracy all known light-based techniques for enhancing the axial resolution. One of the key advantages of this method is that it does not require any hardware modification to a conventional fluorescence-lifetime imaging microscope (FLIM), thus preserving its full lateral resolution. The technical simplicity of MIET and its compatibility with live-cell imaging makes it applicable for broad range of studies.

This chapter partly overlaps with recent review papers that discuss various aspects of MIET imaging [1, 2]. However, in contrast to the previous publications that focus on specific points, such as single molecule imaging using MIET or its comparison with other methods for high resolution axial localization, this chapter provides readers with a general overview of basic principle of MIET and its potential for bio-imaging.

8.2 Basic Principle and Theory

It was predicted by Edward Purcell in 1946 [3] that placing a fluorescent molecule in the vicinity of a metal quenches its fluorescence emission and decreases its excited state lifetime. From a physics point of view, the mechanism behind this phenomenon is similar to that of FRET [4]: energy from the excited molecule is transferred, via electromagnetic coupling, into plasmons of the metal, where energy is either dissipated or re-radiated as light. This fluorophore-metal interaction was extensively studied in the 1970s and 1980s [5], and a quantitative theory developed on the basis of semi-classical quantum optics [6, 7]. The achieved quantitative agreement between experimental measurement and theoretical prediction was excellent (Fig. 8.1).

Owing to the fact that the energy transfer rate is dependent on the distance of a molecule from the metal layer, the fluorescence lifetime can be directly converted into a distance value (Fig. 8.2). The theoretical basis for the success of this conversion is the perfect quantitative understanding of MIET [8]. It is important to emphasize that the energy transfer from the molecule to the metal is dominated by the interaction of the molecule's near-field with the metal and is thus a thoroughly near-field effect,

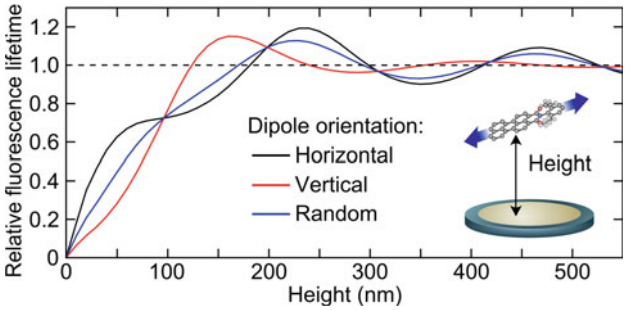

Fig. 8.1 Calculated dependence of fluorophore lifetime on its height over the metal film. Curves are calculated for an emission wavelength of 650 nm and a gold film thickness of 20 nm deposited on the glass substrate

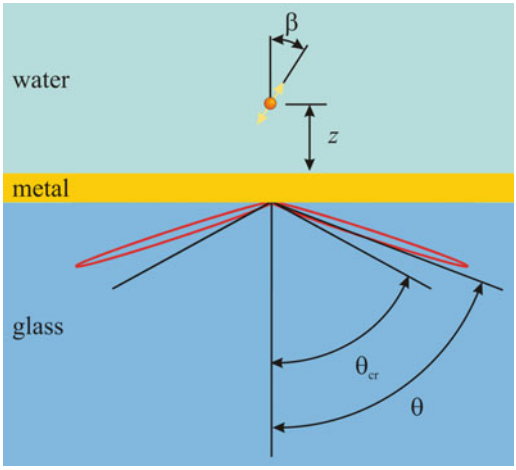

Fig. 8.2 Geometry of MIET sample: A fluorophore is placed above of a thin metal film deposited on glass. Fluorescence detection is done with a high numerical aperture objective lens from the glass side. Fluorescence excitation is performed by the same lens. In the figure, an electric dipole emitter is placed at a distance z from the metal film. Its orientation is described by the angle β between its dipole axis and the optical (vertical) axis. The angular distribution of radiation into the glass is depicted as a red curve and is a function of angle θ. The critical angle θ_{cr} of total internal reflection between glass and water is also shown

similar to FRET. However, due to the planar geometry of the metal film, which acts as the acceptor, the distance dependency of the energy transfer efficiency is much weaker than the sixth power of the distance, which leads to a monotonous relation between lifetime and distance over a size range between zero and ~250 nm above the surface.

Evaluation of MIET measurements can be done by modeling the emission properties of an emitter above a metal surface. The geometry of the modeled situation is shown in Fig. 8.2.

Let us consider the emission of a single molecule with orientation angles (α, β, where β denotes the inclination towards the vertical axis and α the angle around that axis. The molecule is assumed to be an electric dipole emitter. Then, the electric field amplitude of its emission into direction (θ, ϕ) is given by the general formula

$$\mathbf{E}_{em} = \hat{\mathbf{e}}_p \left[A_\perp \cos\beta + A_\parallel^c \sin\beta \cos(\phi - \alpha) \right] + \hat{\mathbf{e}}_s A_\parallel^s \sin\beta \sin(\phi - \alpha) \tag{8.1}$$

where the are functions of emission angle θ but not on α, β or ϕ. Explicit expressions for can be found in a standard way by expanding the electric field of the dipole emission into a plane wave superposition and tracing each plane wave component through the planar structures using Fresnel's relations, for details see [9–12]. It is important to note that the functions depend also on wavelength. Knowing the electric field amplitude of the emission into a given direction (θ, ϕ), one can then derive the total power of emission as

$$S_{\text{total}}(\beta, \alpha) \propto B_\perp \cos^2\beta + B_\parallel \sin^2\beta \tag{8.2}$$

with weight factors $B_{\perp,\parallel}$ which take into account also the absorption of emitted energy within the metal layer, for details of their calculation see [9]. Knowing the total emission power S_{total}, one can then calculate the lifetime of the molecule by

$$\frac{\tau}{\tau_0} = \frac{S_0}{\Phi S_{\text{total}} + 1 - \Phi} \tag{8.3}$$

where S_0 is the total emission power of the emitter in free space (sample space), Φ is the quantum yield, τ_0 is the free space excited state lifetime lifetime of the emitter. For calculating the lifetime-distance curve, one has to average the result over all possible molecular orientations (assuming that there is no preferred molecular orientation in the sample) and the emission spectrum of the emitter (using the free-space emission spectrum as weight function).

Experimentally, one needs a standard scanning confocal microscope that allows one to do fluorescence lifetime imaging (Fig. 8.3), that is, equipped with a pulsed excitation laser and a single photon avalanche diode. The only addition that is required for MIET imaging is coating the substrate with a semitransparent metal film, typically 10–15 nm. Gold as a coating material combines such crucial properties as non-toxicity for living cells, absence of oxidation, and high transparency compared to other metals.

8.3 The MIET-GUI Software

We have developed a Matlab-based MIET-GUI for analysis of measured data. The MIET-GUI is a graphical user interface designed for various types of data evaluation, for instance the conversion of the raw FLIM data into a MIET image. The software

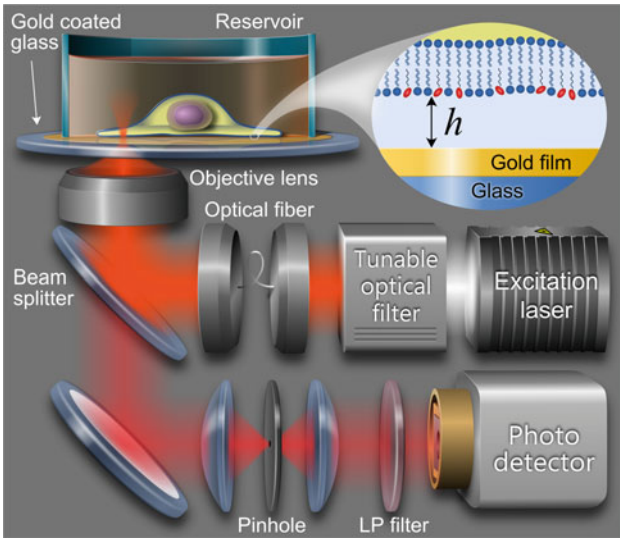

Fig. 8.3 Schematic of the experimental set-up for MIET imaging

can be downloaded via the link www.joerg-enderlein.de/MIET/MIETGUI.zip. The MIET-GUI accepts .ht3 and .ptu files generated by the FLIM-hardware HydraHarp of PicoQuant GmbH (Berlin), from which it calculates the lifetime and intensity for every pixel of an image, elliptical regions of interest (ROI) or the patterns generated by scanning the excitation light over single dipole emitters. These lifetimes are converted into height information via the MIET lifetime versus height calibration curve (Fig. 8.4).

As a first step, the user has to choose the general type of evaluation, pixel-by-pixel or one of the more elaborate ROI/pattern techniques. In the pixel-by-pixel mode, the time-correlated single photon counting (TCSPC) histogram of each pixel with more than 25 photons is assembled. The shape of these histograms can be described by a steep rise followed by a peak and then an exponential decay. By setting a cutoff after which the curve is purely exponential and calculating the mean arrival time of the photons after this cutoff, one gets the lifetime value for this pixel. In the ROI mode, the user specifies an elliptical region of interest believed to belong to molecules with the same lifetime. The photons from all pixels within the ROI are collected into a single histogram, which is less prone to noise problems than histograms for single pixels. For this reason, the histogram can be fit with either mono- or multi-exponential decay curves, thus finding the lifetime of the molecules in the ROI. The most sophisticated mode is the pattern matching mode. Here, the user has to specify the parameters of the excitation light such as the wavelength, the polarization mode of the laser, the numerical aperture of the objective and the defocusing of the objective. From these parameters, the patterns generated by scanning the excitation beam over molecules with different angular orientations can be calculated. The intensity image obtained by integrating the TCSPC data over time is now fitted with the simulated

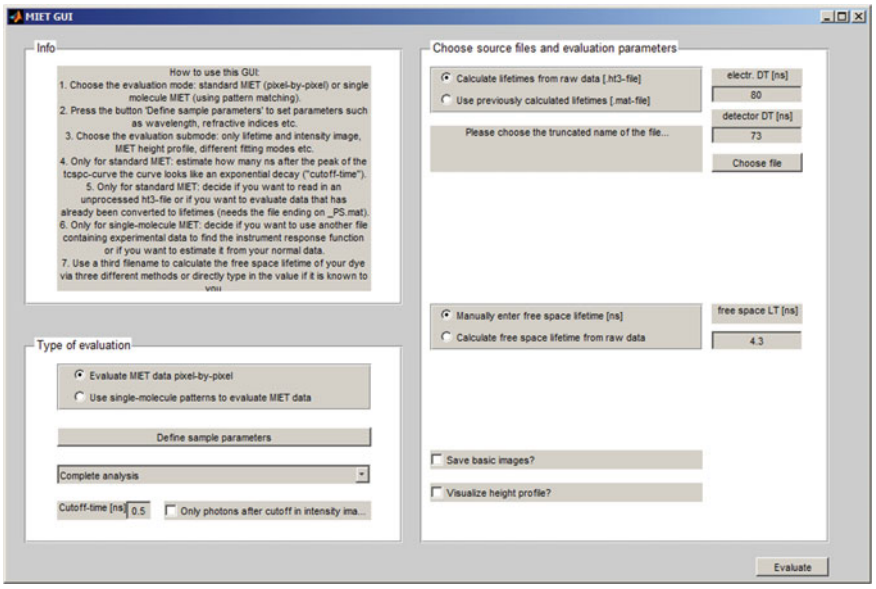

Fig. 8.4 Interface of the Matlab-based MIET-GUI software for the analysis of raw data

patterns to determine the position and orientation of each single dipole emitter. The photons from all the pixels assigned to a molecule's pattern are grouped into a single histogram and fitted as in the ROI mode.

In the second step, the lifetime information is converted into height information. To this end, the user has to specify the emission wavelength, the quantum yield and the excited state lifetime of the emitters as well as the thicknesses and complex refractive indices of all materials in the sample (e.g. metal-coated glass cover slides, buffer solutions etc.). As described above, this data can be used to calculate the observed lifetime as a function of the dipole's height above the interface and its angle with the optical axis. In the pixel-by-pixel evaluation mode, nothing is known about the particle's orientation, so a random orientation is assumed and the calibration curve calculated accordingly. In the pattern matching mode, the particle's orientation is known and the correct curve is used for the evaluation. If the emission spectrum of the fluorescent probe is known, the calibration curves obtained for all wavelengths that are able to pass the optical filters are calculated and averaged according to the spectrum. A complication arises from the fact that the lifetime versus height curve oscillates, meaning that some lifetime values cannot be matched unambiguously to a height value. The first possibility for solving this problem is to crop the calibration curve at the largest unique value and to mark all longer lifetimes as 'not a number' in the height image. If there is a prior knowledge about the sample states that no height values larger than the value corresponding to the first peak in the calibration curve can exist, it is possible to crop the calibration curve at this peak. The height information gained through this progress can then be visualized or used for further analysis.

8.4 Metal-Induced Energy Transfer for Biological Imaging

The applicability of MIET for live-cell imaging has been first shown by mapping the basal membrane of living cells with nanometer accuracy [13]. Knowledge of the precise cell-substrate distance as a function of time and location with unprecedented resolution provides a new means to quantify cellular adhesion and dynamics, as is required for a deeper understanding of fundamental biological processes such as cell differentiation, tumor metastasis and cell migration.

As a biological model system three adherent cell lines were chosen: MDA-MB-231 human mammary gland adenocarcinoma cells and A549 human lung carcinoma cells, which are able to form metastasis in vivo models, as well as MDCK-II from canine kidney tissue as a benign epithelial cell line. Interestingly, significant differences in the cell–interface distance between a normal epithelial cell and cancerous cell lines were observed.

Figure 8.5a and b show the measured intensity and lifetime images that were used to obtain the 3D reconstruction of the basal cell membrane. Because the variation of the fluorescence intensity is not only dependent on the metal-induced quenching, but also on the homogeneity of labelling, exclusively the lifetime information was used for reconstructing a three-dimensional map of the basal membrane. On the other hand, the intensity distribution was used to discriminate the membrane fluorescence against the background. Regions with no cells are difficult to identify from the lifetime images alone, as the lifetime values can become exceedingly scattered at low signal-to-noise ratios. Figure 8.5c shows the result of recalculation of the lifetime image into the 3d height profile.

A relatively fast scanning speed of a confocal microscope that is used for MIET imaging allows to monitor dynamic processes. Figure 8.6 shows the spreading behaviour of MDCK-II cells. Generally, the spreading process of adherent cells can be divided into three distinct temporal phases. The first phase is characterized by the formation of initial bonds between adhesion molecules and molecules of the extracellular matrix. This process of tethering is followed by the second phase, which

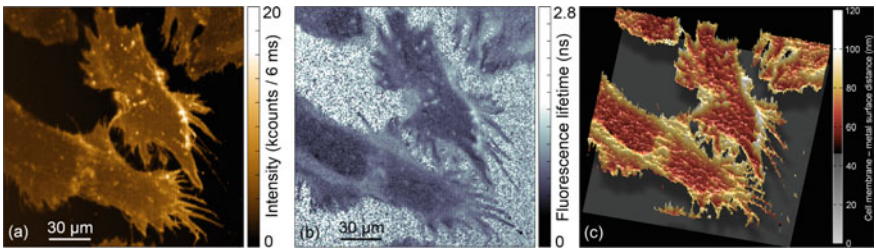

Fig. 8.5 Simultaneously acquired fluorescence intensity (**a**) and lifetime (**b**) images of the basal membrane of living MDA-MB-231 cells grown on a gold-covered glass substrate, acquired with a standard confocal microscope. **c** Three-dimensional reconstruction of the basal cell membrane. Three-dimensional profiles computed from the fluorescence lifetime image (**b**)

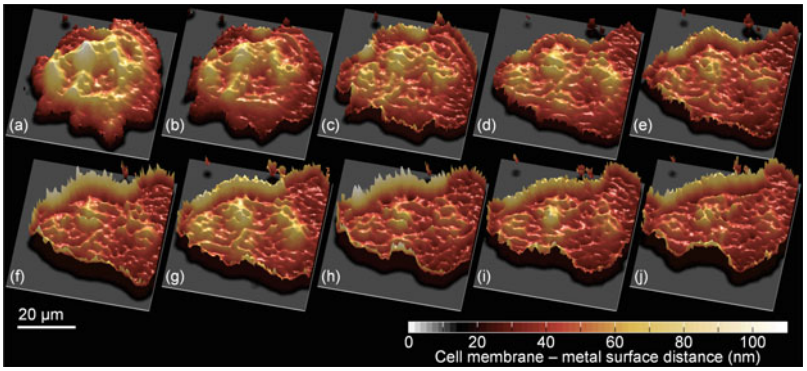

Fig. 8.6 Time elapsed MIET images recorded in 5 min time intervals showing the late stages of cell (MDCK-II) spreading on gold. The cell forms tightly attached protrusions/lamellipodia away from the center of the cell. The cell occupies a larger area with time and presses down more closely. A darker color refers to lower cell-substrate distance. At later stages (k-n) first lamellipodia are formed that exhibit a low cell-substrate distance

comprises the initial cell spreading and that is driven by actin polymerization. The latter forces the cell surface area to increase by drawing membrane from a reservoir of folded regions. The third phase encompasses recruitment of additional plasma membrane from the internally stored membrane buffer and extension of lamellipodia to occupy a larger area.

The axial resolution of the recorded images can be determined by calculating the standard deviation of cell-substrate distance. The resolution depends on the photon rate and varies between 2 and 4 nm for typical fluorescence intensities measured and can be further enhanced to 1 nm by increasing the number of detected photons.

The unprecedented axial resolution of MIET allowed us to monitor the cell-substrate distance of epithelial NMuMG cells during the biological process of the epithelial-tomesenchymal transition (Fig. 8.7) [14]. EMT allows epithelial cells to enhance their migratory and invasive behavior and plays a key role in embryogenesis, fibrosis, wound healing, and metastasis. Among the multiple biochemical changes from an epithelial to a mesenchymal phenotype, the alteration of cellular dynamics in cell-cell as well as cell-substrate contacts is crucial. It was shown that, in the very first hours of the transition, the cell-substrate distance increases by several tens on nanometers, but later in the process after reaching the mesenchymal state, this distance is reduced again to the level of untreated cells.

Dual-color MIET allowed for reconstructing the 3D profile of the nuclear envelope over the whole basal area of HeLa cells [15]. The profilometry was done by measuring the axial distance between the proteins Lap2β and Nup358 as components of the nuclear envelope and the nuclear pore complex, with defined localizations at the inner nuclear membrane and the cytoplasmic side of the protein complex, respectively (Fig. 8.8). The obtained thickness of the nuclear envelope of 30–35 nm is in very good agreement with the values that were obtained using electron microscopy. This study

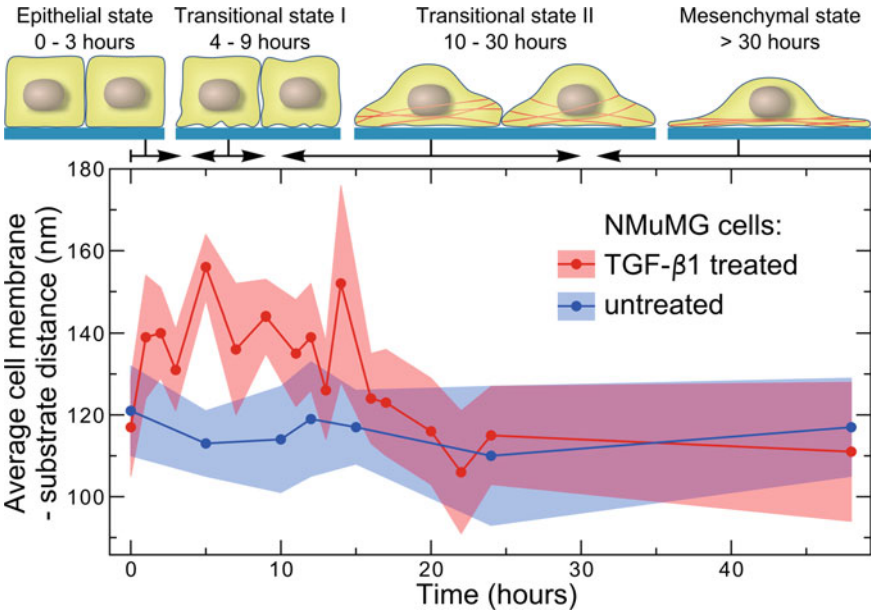

Fig. 8.7 Average cell membrane-substrate distance of untreated (blue) and TGF-β1 treated NMuMG cells (red) over time. NMuMG cells detach from the surface by more than 20 nm on average in response to TGF-β1 administration. After 20 h the initial cell-substrate distance is restored. The standard error of mean is illustrated as colored area around the data points

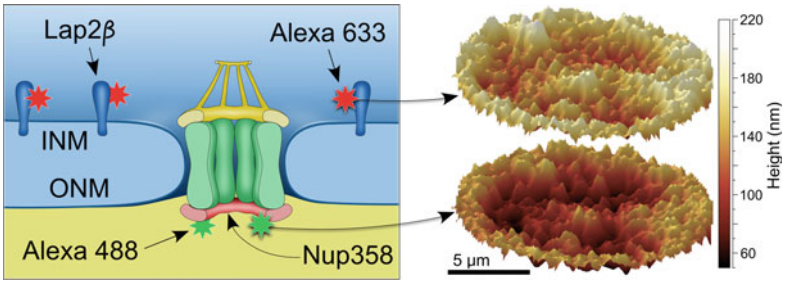

Fig. 8.8 Schematic of the positions of Lap2β and Nup358 in the inner nuclear membrane and the nuclear pore complex, respectively. HeLa cells were fixed and subjected to indirect immunofluorescence using goat anti-Nup358. Three-dimensional height profiles of the inner (top) and outer (bottom) nuclear membrane of a typical HeLa cell nucleus, as determined by MIET imaging. The outer nuclear membrane roughly follows the profile of the inner nuclear membrane

has shown that optical microscopy allows one not only to measure the distance between the outer and inner nuclear membrane but also to reconstruct its 3D profile over the whole basal area.

Recently, dual-color MIET was combined with Förster resonance energy transfer (FRET) for studies of cytoskeletal elements and adhesions in human mesenchymal

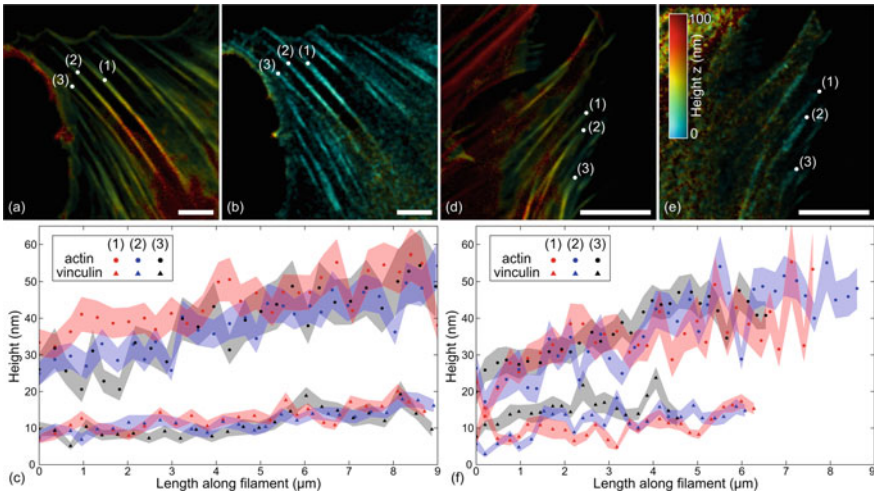

Fig. 8.9 3D architecture of stress fibers at focal adhesions changes from 12 to 24 h. Height profiles along actin filaments and vinculin complexes after 12 and 24 h. Images a and b correspond to intensity-weighted ensemble heights of actin and vinculin, respectively, for a cell fixed 12 h after seeding. Images d and e correspond to intensity-weighted ensemble heights of actin and vinculin, respectively, for a cell fixed 24 h after seeding. White points (1), (2), and (3) on the intensity-weighted height images indicate the starting points of the height profiles shown in images (**c**) and (**f**). They show the height of actin filaments (circles) and vinculin clusters (triangles) at the same focal adhesion. The shaded areas mark the 1σ-regions of the height values. Scale bar is 10 μm

stem cells [16]. In addition to resolving nanometric structural details along the z-axis using MIET, FRET was used to measure the distance between actin and vinculin at focal adhesions. The analysis of the temporal evolution of actin heights shows that the actin filaments move closer to the surface while the cell is spreading and firmly adhering (Fig. 8.9). Although the fibers are distributed over a broad height range during an early phase (1–6 h), their distance to the surface reduces around 12 h and later time points to 40 nm. On the other hand, during maturation of focal adhesion complexes, vinculin aggregates grow larger as indicated by an increase in height, and the mean height of the actin bundles above the surface is decreasing. The nanometer-precise height information along the fibers and of the vinculin clusters Fig. 8.9 gives a detailed picture of stress fibers anchoring at focal adhesions and spanning the cell at a slight inclination of below 1°.

Use of single photon counting detectors for MIET measurements allow one not only to achieve nanometer resolution of sub-cellular structures with high labeling density, but also to do nanometer axial localization of single molecules. The proof of principle study was done by Karedla et al., where the authors determined the height of dye molecules deposited on a dielectric spacer of a known thickness [17]. By varying the thickness of the spacer, the authors showed that the axial position of molecules can be determined with accuracy better than 2.5 nm. The excellent agreement between the known thickness and the height values that were obtained

using MIET showed its applicability for single molecule studies with accuracy that unachievable with conventional microscopy techniques.

Isbaner et al. used MIET for colocalizing two single fluorescent emitters along the optical axis with nanometer accuracy [18]. For this purpose, the authors used stepwise photobleaching to find the fluorescence lifetime values of each emitter on one DNA origami pillar, which allowed them to determine their individual heights from the surface and thus their mutual axial distance. The determined distance of 32 ± 11 nm is in excellent agreement with the design value of 32 nm.

8.5 Conclusions

The review of applications of MIET shows its versatility and potential for numerous application in live cell imaging and single molecule localization. The unique combination of its technical simplicity and nanometer axial resolution makes it widely applicable for numerous studies in life science or nanotechnology. The distance range covered by MIET nicely bridges (and complements) the realm of conventional FRET and all the recently developed super-resolution imaging techniques. It opens new perspectives for nanometer localization of sub-cellular structures in cell focal adhesion complexes. Since MIET keeps all the key advantages of conventional fluorescence microscopy, it allows to do simultaneous multi-color imaging of various sub-cellular structures. Extremely high photo-sensitivity of single photon avalanche diodes that are used as photo-detectors for MIET imaging allow one to singe molecule localization with precision that in unimaginable for conventional optical microscopy. We envision further rapid growth of the number of its applications and technical development for increasing its temporal and spatial resolution.

Acknowledgements We are grateful to the Deutsche Forschungsgemeinschaft (DFG) for financial support via project A05 of the SFB755 and project A14 of the SFB937 as well as through the Cluster of Excellence and DFG Research Center "Nanoscale Microscopy and Molecular Physiology of the Brain."

References

1. Chizhik, A. I.: Super-Resolution Depth Measurements: variable Angle TIRF, Super-Critical Angle Fluorescence, MIET, pp. 175–184. Elsevier (2018). https://doi.org/10.1016/B978-0-12-803581-8.09496-0., https://doi.org/10.1007/4243_2014_77
2. Karedla, N., Ruhlandt, D., Chizhik, A.M., Enderlein, J., Chizhik, A.I.: Metal-Induced Energy Transfer, pp. 265–281. Springer International Publishing (2015). https://doi.org/10.1007/4243_2014_77
3. Purcell, E.M.: Spontaneous emission probabilities at radio frequencies. Phys. Rev. **69**, 681 (1946)

4. Ha, T., Enderle, T., Ogletree, D., Chemla, D.S., Selvin, P.R., Weiss, S.: Probing the interaction between two single molecules: fluorescence resonance energy transfer between a single donor and a single acceptor. Proc. Natl. Acad. Sci. **93**(13), 6264–6268 (1996)
5. Drexhage, K.H.: Iv Interaction of Light with Monomolecular Dye Layers. pp. 163–232. Elsevier (1974). https://doi.org/10.1016/S0079-6638(08)70266-X
6. Chance, R.R., Prock, A., Silbey, R.: Molecular Fluorescence and Energy Transfer Near Interfaces, pp. 1–65. Wiley-Blackwell (2007). https://doi.org/10.1002/9780470142561.ch1
7. Lukosz, W., Kunz, R.E.: Light emission by magnetic and electric dipoles close to a plane interface. i. total radiated power. J. Opt. Soc. Am. **67**(12), 1607–1615 (1977). https://doi.org/10.1364/JOSA.67.001607, http://www.osapublishing.org/abstract.cfm?URI=josa-67-12-1607
8. Enderlein, J.: Theoretical study of single molecule fluorescence in a metallic nanocavity. Appl. Phys. Lett. **80**(2), 315–317 (2002). https://doi.org/10.1063/1.1434314
9. Enderlein, J.: Single-molecule fluorescence near a metal layer. Chem. Phys. **247**(1), 1–9 (1999). https://doi.org/10.1016/S0301-0104(99)00097-X
10. Enderlein, J.: A theoretical investigation of single-molecule fluorescence detection on thin metallic layers. Biophys. J. **78**(4), 2151–2158 (2000). https://doi.org/10.1016/S0006-3495(00)76761-0
11. Enderlein, J., Ruckstuhl, T.: The efficiency of surface-plasmon coupled emission for sensitive fluorescence detection. Opt. Express **13**(22), 8855–8865 (2005). https://doi.org/10.1364/OPEX.13.008855, http://www.opticsexpress.org/abstract.cfm?URI=oe-13-22-8855
12. Enderlein, J., Ruckstuhl, T., Seeger, S.: Highly efficient optical detection of surface-generated fluorescence. Appl. Opt. **38**(4), 724–732 (1999). https://doi.org/10.1364/AO.38.000724, http://ao.osa.org/abstract.cfm?URI=ao-38-4-724
13. Chizhik, A.I., Rother, J., Gregor, I., Janshoff, A., Enderlein, J.: Metal-induced energy transfer for live cell nanoscopy. Nat. Photonics **8**(2), 124 (2014)
14. Baronsky, T., Ruhlandt, D., Brückner, B.R., Schäfer, J., Karedla, N., Isbaner, S., Hühnel, D., Gregor, I., Enderlein, J., Janshoff, A., Chizhik, A.I.: Cell-substrate dynamics of the epithelial-to-mesenchymal transition. Nano Lett. **17**(5), 3320–3326 (2017)
15. Chizhik, A.M., Ruhlandt, D., Pfaff, J., Karedla, N., Chizhik, A.I., Gregor, I., Kehlenbach, R.H., Enderlein, J.: Three-dimensional reconstruction of nuclear envelope architecture using dual-color metal-induced energy transfer imaging. ACS Nano **11**(12), 11839–11846 (2017). https://doi.org/10.1021/acsnano.7b04671. PMID: 28921961
16. Chizhik, A.M., Wollnik, C., Ruhlandt, D., Karedla, N., Chizhik, A.I., Hauke, L., Hähnel, D., Gregor, I., Enderlein, J., Rehfeldt, F.: Dual-color metal-induced and förster resonance energy transfer for cell nanoscopy. Mol. Biol. Cell **29**(7), 846–851 (2018)
17. Karedla, N., Chizhik, A.M., Stein, S.C., Ruhlandt, D., Gregor, I., Chizhik, A.I., Enderlein, J.: Three-dimensional single-molecule localization with nanometer accuracy using metal-induced energy transfer (miet) imaging. J. Chem. Phys. **148**(20), 204,201 (2018)
18. Isbaner, S., Karedla, N., Kaminska, I., Ruhlandt, D., Raab, M., Bohlen, J., Chizhik, A., Gregor, I., Tinnefeld, P., Enderlein, J., et al.: Axial colocalization of single molecules with nanometer accuracy using metal-induced energy transfer. Nano Lett. **18**(4), 2616–2622 (2018)